

Review

Sensitive Electrochemical Detection of Bioactive Molecules (Hydrogen Peroxide, Glucose, Dopamine) with Perovskites-Based Sensors

Imane Boubezari ¹, Ali Zazoua ¹ , Abdelhamid Errachid ² and Nicole Jaffrezic-Renault ^{2,*} 

¹ Laboratory of Applied Energetics and Materials, University of Jijel, Ouled Aissa 18000, Algeria; boubezari.imen@gmail.com (I.B.); a_zazoua@univ-jijel.dz (A.Z.)

² Institute of Analytical Sciences, University of Lyon, 69100 Villeurbanne, France; abdelhamid.errachid-el-salhi@univ-lyon1.fr

* Correspondence: nicole.jaffrezic@univ-lyon1.fr

Abstract: Perovskite-modified electrodes have received increasing attention in the last decade, due to their electrocatalytic properties to undergo the sensitive and selective detection of bioactive molecules, such as hydrogen peroxide, glucose, and dopamine. In this review paper, different types of perovskites involved for their electrocatalytic properties are described, and the proposed mechanism of detection is presented. The analytical performances obtained for different electroactive molecules are listed and compared with those in terms of the type of perovskite used, its nanostructuring, and its association with other conductive nanomaterials. The analytical performance obtained with perovskites is shown to be better than those of Ni and Co oxide-based electrochemical sensors. Main trends and future challenges for enlarging and improving the use of perovskite-based electrochemical sensors are then discussed.

Keywords: perovskite; voltammetry; hydrogen peroxide; glucose; dopamine



Citation: Boubezari, I.; Zazoua, A.; Errachid, A.; Jaffrezic-Renault, N. Sensitive Electrochemical Detection of Bioactive Molecules (Hydrogen Peroxide, Glucose, Dopamine) with Perovskites-Based Sensors.

Chemosensors **2021**, *9*, 289.

<https://doi.org/10.3390/chemosensors9100289>

<https://doi.org/10.3390/chemosensors9100289>

Academic Editor: Paolo Ugo

Received: 7 September 2021

Accepted: 5 October 2021

Published: 12 October 2021

Publisher's Note: MDPI stays neutral with regard to jurisdictional claims in published maps and institutional affiliations.



Copyright: © 2021 by the authors. Licensee MDPI, Basel, Switzerland. This article is an open access article distributed under the terms and conditions of the Creative Commons Attribution (CC BY) license (<https://creativecommons.org/licenses/by/4.0/>).

1. Introduction

For the integration in point-of-care testing (POCT) systems [1], such as commercial kits available for monitoring patients' glucose levels (i.e., Accu-Chek® from Roche Diabetes Care Company) [2], there is an urgent need for precise, sensitive, portable, and cost-effective technologies for the detection of bioactive molecules. In this group of chemical compounds, hydrogen peroxide is a cancer biomarker, because, in comparison to normal cells, cancer cells are characterized by an increased H₂O₂ production rate and an impaired redox balance, thereby affecting the antitumoral immune response [3]. Diabetes mellitus is due to an abnormal level of glucose in the blood, and this level should be frequently monitored [4]. Dopamine (DA) is one of the most important catecholamines, present in the human central nervous system. Its depletion that should be monitored leads to neurodegenerative diseases such as Parkinson's disease [5].

Electrochemical sensors are good candidates for their integration in POCT systems [6], due to their easy miniaturization and the low-cost instrumentation that could be interfaced with smart phones. All these bioactive molecules can be sensitively detected by enzymatic electrochemical sensors [7–9]. The main drawback of these enzymatic sensors is the stability of enzymes and their activities being modified by the immobilization procedure, by the pH value, or by the presence of inhibiting agents. The use of non-enzymatic electrochemical sensors should be highly required. During the last decade, perovskite nanomaterials have shown electrocatalytic properties, and bioactive molecules could be easily sensitively and selectively detected using perovskite-based electrodes, which present the advantage of stability of the sensors.

Perovskite oxides were discovered by Gustav Rose in the Ural mountains in 1839; the most common formula of perovskites is ABO₃, with A being an alkali metal or a lanthanide,

B being a transition metal, and O being the oxygen ion. The charges of A and B ions should be equivalent to the whole charge of the oxygen ions. The tolerance factor should be in the range of 0.8–1.0 with the radii of A and B ions greater than 0.090 nm and 0.051 nm, respectively. The cubic structure of the perovskite is stabilized by the 6-fold coordination of the B cation and the 12-fold coordination of the A cation (Figure 1).

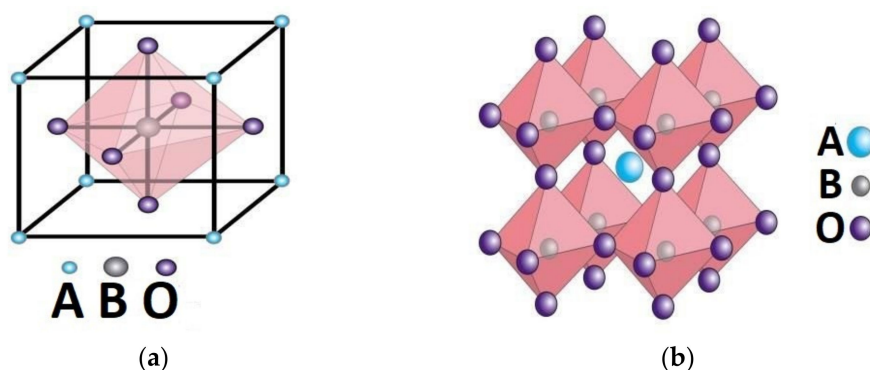


Figure 1. (a) Cubic mesh of perovskite; (b) three-dimensional (3D) stacking in the ideal cubic structure.

Some distortions may occur in the ideal cubic structure, leading to orthorhombic, tetragonal, rhombohedral, or hexagonal structures.

Perovskite oxides present a diversity of electrical properties from insulating to semi-conducting metallic and superconducting properties. They also present magnetic and optical properties [10]. A lot of devices are then conceived from perovskite oxides: photochromic, electrochromic, image storage, switching, filtering, and surface acoustic wave signal-processing devices. In addition, they have been used as catalysts in different applications such as engine-exhaust gas treatment and hydrogen evolution reaction.

Several recent review papers were devoted to the sensory applications of perovskite based on their electrical and of optical properties [11–17]. This review paper is based on an exhaustive list of perovskite-based electrochemical sensors for the enzyme-free detection of hydrogen peroxide, glucose, and DA. In each case, the involved mechanism is described, and the analytical performance of the obtained sensor is presented. The perovskite formula leading to the lowest detection limit is highlighted, as well as the one leading to the most selective detection. The improvement brought by the association with other nanomaterials is also shown. The analytical performance of the perovskite-based sensors and those of nickel oxide and cobalt oxide-based sensors are compared. The main trends and future challenges are discussed.

2. Methods for the Synthesis and Characterization of Perovskites

2.1. Sol-Gel Synthesis

The sol-gel synthesis of precursors is one of the procedures used for the synthesis of perovskites [18]. It is based on the Pechini method that involves two chemical reactions: with nitrate salts of the metal ions being mixed according to the stoichiometry, the complexation of metal ions occurs with the addition of citric acid, and the polyesterification of the complexes is obtained with the addition of ethylene glycol [19]. A viscous solution is obtained after heating to 130 °C in an argon flow under stirring for about 10 h. The temperature is then raised to 150–200 °C to obtain a foam-dried mass which has to be ground in a mortar. This precursor is calcined at different temperatures of 600, 850, and 1000 °C in a muffle furnace, depending on the final targeted product.

2.2. Microwave Irradiation Process

The microwave irradiation process shows many advantages such as rapid reaction velocity, uniform heating, cleanness, and high energy efficiency. The conditions used for microwave preparation are 2.45 GHz, with a maximum output power of not less than

1 kW. Dielectric materials can absorb the microwave energy and transform it into heat energy directly through polarization and dielectric loss in the interior of the materials. Single-phase manganese-based perovskites are simply obtained from nitric solutions by a denitration process under microwave irradiation [20].

2.3. Coprecipitation Process

In the coprecipitation process [18], different types of precursors are employed: oxides, alkoxides, inorganic salts, and nitrates. The processing parameters (pH, coprecipitation rate, washing, drying, and temperature of synthesis) are controlled which results in homogeneous and weakly agglomerated nanopowders. They can be sintered at temperatures as low as 1250 °C and for short times (1–2 h) for the obtaining of perovskites of near the theoretical density.

2.4. Solid-State Synthesis Technique

LaFeO₃ nanoparticles are prepared through the solid-state synthesis technique using mechanical ball milling [21]. Stoichiometric amounts of La₂O₃ and Fe₂O₃ metal oxide precursors (molar ratio: 1:1) are transferred to a planetary ball mill. Wet milling is carried out for 20 h (with toluene as the process control agent). Based on thermal analysis, the ball milled powder is calcined at 900 °C for 2 h and then ground into fine powders in an agate mortar and pestle.

2.5. Other Synthesis Techniques

LaNiO₃ electrospun nanofibers are prepared by mixing metal salts with polyvinylpyrrolidone (PVP) followed by sequential calcinations [22]. Thin films of La_{0.5}Sr_{0.5}CoO_{3-δ} are obtained by the pulsed laser deposition (PLD) technique [23].

2.6. Characterization Methods

The different phases of the prepared perovskites can be differentiated using X-ray powder diffraction (XRD). In addition, the structure of perovskite can be characterized using single-crystal XRD analysis. Thermal analysis techniques such as thermogravimetry (TGA), differential thermal analysis (DTA), and differential scanning calorimetry (DSC) can be used to test the thermal stability of the prepared perovskites. The different morphological characteristics of the prepared perovskites can be studied using scanning electron microscopy (SEM) and transmission electron microscopy (TEM). In addition, the surface area measurement of the prepared perovskites can be carried out using surface area analysis (BET). Raman spectroscopy allows the determination of vibration modes in relation with molecular dynamics. In addition, the surface chemical groups of the prepared perovskites can be identified using Fourier-transform infrared spectroscopy (FTIR) and X-ray photoelectron spectroscopy (XPS). The frequency-dependent conductivity spectra are determined by using impedance spectroscopy.

3. Perovskite-Based Electrochemical Sensors for the Detection of Hydrogen Peroxide

Table 1 shows a summary of Perovskite-based electrochemical sensors for the detection of hydrogen peroxide.

Table 1. Perovskite-based electrochemical sensors for the detection of hydrogen peroxide.

Type of Perovskite Electrode	Perovskite Preparation	Sensitivity	Linear Range	Detection Limit (LOD)	Lifetime	Applications	References
$\text{Sr}_{0.85}\text{Ce}_{0.15}\text{FeO}_3$ Perovskite + Nafion®/SPE	citrate-nitrate smoldering autocombustion	60 $\mu\text{A}/\text{mM}/\text{cm}^2$	0–500 μM	10 μM	12 months		[24]
SmCoO_3 Perovskite + conductive carbon + Nafion®/GCE	EDTA-citrate complexing sol-gel + calcination	715 $\mu\text{A}/\text{mM}/\text{cm}^2$	0.1–5000 μM	0.004 μM			[25]
$\text{La}_{0.6}\text{Ca}_{0.4}\text{MnO}_3$ CPE	Malic acid—nitrate Sol-gel method + calcination		0–0.5 mM				[26]
$\text{La}_{0.7}\text{Sr}_{0.3}\text{Mn}_{0.75}\text{Co}_{0.25}\text{O}_3$ CPE	Metal salts mixed with polyvinylpyrrolidone (PVP) Electrospinning and calcination	1371 $\mu\text{A}/\text{mM}$	0.5–1000 μM	0.17 μM	30 days	Toothpaste Medical hydrogen peroxide	[27]
$\text{LaNi}_{0.6}\text{Co}_{0.4}\text{O}_3$ CPE	Citrate-nitrate Sol-gel method + calcination	1812 $\mu\text{A}/\text{mM}/\text{cm}^2$	10 nM–100 μM	1 nM	20 days	Toothpaste	[28]
$\text{Co}_{0.4}\text{Fe}_{0.6}\text{LaO}_3$ CPE	Citrate-nitrate Sol-gel method	2376.7 nA/ μM	0.01–800 μM	2 nM	3 weeks		[29]
$\text{La}_{0.66}\text{Sr}_{0.33}\text{MnO}_3$ CPE	Microwave irradiation of nitric solution	1770 $\mu\text{A}/\text{M}$				Cleaning product	[20]
LaNiO_3 CPE	Metal salts mixed with PVP Electrospun nanofibers	1135.88 $\mu\text{A}/\text{mM}/\text{cm}^2$	0.05–1000 μM	33.9 nM	4 weeks		[22]
$\text{LaNi}_{0.5}\text{Ti}_{0.5}\text{O}_3/\text{CoFe}_2\text{O}_3$ GCE	Citrate-nitrate Sol-gel method + calcination	3.21 $\mu\text{A}/\text{mM}/\text{cm}^2$	0.1 μM –8.2 mM	23 nM	4 weeks	Toothpaste	[30]
$\text{La}_{0.6}\text{Sr}_{0.4}\text{Co}_{0.2}\text{Fe}_{0.8}\text{O}_{3-\delta}$	Citrate-nitrate Sol-gel method + calcination	580 $\mu\text{A}/\text{mM}/\text{cm}^2$	0 mM	5 μM			[31]
$\text{La}_{0.5}\text{Sr}_{0.5}\text{CoO}_{3-\delta}$ E-MOSFET	Pulsed laser deposition technique			1 mM			[23]
$\text{La}_{0.6}\text{Sr}_{0.4}\text{CoO}_{3-\delta}$ Perovskite + Nafion®/GCE	EDTA-citrate complexing sol-gel + calcination	280 $\mu\text{A}/\text{mM}/\text{cm}^2$	0.4–3350 μM	0.12 μM			[32]
$\text{La}_{0.6}\text{Sr}_{0.4}\text{CoO}_{3-\delta}$ Perovskite + RGO + Nafion®/GCE	EDTA-citrate complexing sol-gel + calcination	500 $\mu\text{A}/\text{mM}/\text{cm}^2$	0.2–3350 μM	0.05 μM			[32]
LaMnO_3 /conductive carbon black GCE	Precipitation method + calcination + carbon coating	897.6 $\mu\text{A}/\text{mM}/\text{cm}^2$	5–5550 μM	0.807 nM	30 days		[33]
Nafion- LaNiO_3 GCE	Citrate-nitrate Sol-gel method + calcination		0.2 μM –50 μM	35 nM		Serum samples	[34]

The first study about the electrochemical detection of hydrogen peroxide using a perovskite was published in 1996 by Shimizu [26]. Among ABO_3 perovskites used for the electrochemical detection of hydrogen peroxide (Table 1), the more commonly used are lanthanum-based perovskites, certain being substituted with alkaline earth ions such as calcium and strontium. The frequency of the use of B ions for the H_2O_2 detection, among all the published papers (Table 1), is as follows: $Co > Ni = Mn > Fe > Ti$. A-site ion is mainly La that can be substituted by alkaline ions such as strontium [20,23,27,31,32] or calcium [26].

Figure 2 illustrates the overall steps of the H_2O_2 electro-oxidation on the perovskite surface, which involves diffusion, adsorption/desorption, and electro-oxidation reaction.

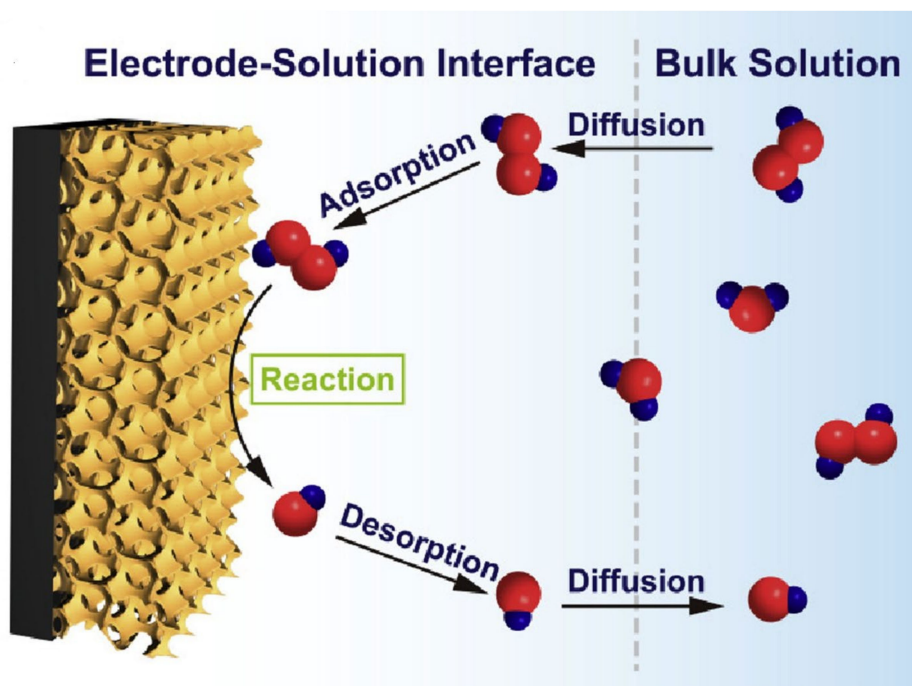


Figure 2. Schematic diagram of the overall process steps on a perovskite/glassy carbon electrode (GCE) [21]. Reproduced with the permission from Elsevier.

The complex mechanisms involved in the electrocatalytic oxidation of hydrogen peroxide were deeply analyzed [32]. The partial substitution of the A-site cations by divalent cations such as Ca^{2+} , Sr^{2+} , and Ba^{2+} can lead to an oxidation of the B-site cation as B^{3+} [24,25,27,32]. The increasing of this substitution also leads to the reduction in oxygen vacancy formation energy which is consistent with the existence of highly oxidative oxygen species [32]. The most possible mechanism of the oxidation of H_2O_2 on $La_{0.6}Sr_{0.4}CoO_{3-\delta}$ in 0.1 M NaOH at a potential of 0.3V/Ag/AgCl is presented in Figure 3. Two parallel pathways are involved: Co^{3+}/Co^{4+} redox couple (Figure 3A) and oxygen vacancies formation which allows the transfer of lattice oxygen to the adsorbed intermediates, generating ion superoxide (defined as the lattice-oxygen-mediated oxygen evolution reaction (LOM-OER); Figure 3B).

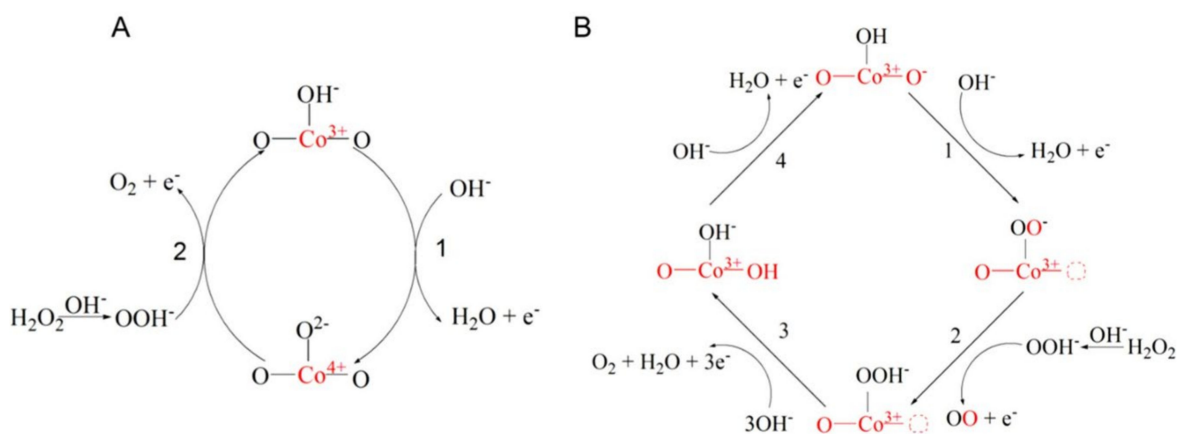


Figure 3. Electro-oxidation mechanisms of H_2O_2 on $\text{La}_{0.6}\text{Sr}_{0.4}\text{CoO}_{3-\delta}$ that occur simultaneously via the $\text{Co}^{3+}/\text{Co}^{4+}$ redox couple (A) and lattice-oxygen-mediated oxygen evolution reaction (LOM-OER) (B) involving oxygen vacancies and superoxide ion ($\text{O}_2^{\cdot-}/\text{O}^-$) [32]. Reproduced with the permission from Elsevier.

Regarding the analytical performance of the perovskite-based electrochemical sensors for H_2O_2 , the obtained lower detection limits are 1 nM and 2 nM, obtained with $\text{LaNi}_{0.6}\text{Co}_{0.4}\text{O}_3$ and with $\text{LaCo}_{0.4}\text{Fe}_{0.6}\text{O}_3$, respectively [28,29].

The specific surface area of the perovskite can be increased by different preparation procedures, showing that this parameter is also of importance for the analytical performance. Electrospun nanofibers are prepared by mixing $\text{La}_{0.7}\text{Sr}_{0.3}\text{Mn}_{0.75}\text{Co}_{0.25}\text{O}_3$ [27] and with LaNiO_3 [22] in PVP. Higher sensitivities of detection (more than $1000 \mu\text{A}/\text{mM}/\text{cm}^2$) and large dynamic ranges until $1000 \mu\text{M}$ are obtained. A three-dimensional (3D) ordered microporous SmCoO_3 perovskite is prepared using a poly(methylmethacrylate) colloidal crystal template route [25]. A detection limit of 4 nM and a dynamic range from 0.1 to $5000 \mu\text{M}$ are obtained.

The association of perovskites with conductive nanomaterials allows a decrease of the detection limit. When perovskite LaMnO_3 is intimately mixed with a conductive carbon black, forming a composite, a very low detection limit of 0.805 nM is obtained. [33]. It was also noticed that the mixture of $\text{La}_{0.6}\text{Sr}_{0.4}\text{CoO}_{3-\delta}$ with reduced graphene oxide [32] improves the sensitivity by a factor of 2 and decreases the detection limit also by a factor of 2.

The storage stability of these perovskite-based sensors is in the range of one month.

4. Perovskite-Based Electrochemical Sensors for the Detection of Glucose

As for hydrogen peroxide detection, numerous works on the detection of glucose (Table 2) are carried out using La-based perovskites. In some of them, La is substituted by alkaline earth such as strontium [31,32].

Table 2. Perovskite-based electrochemical sensors for the detection of glucose.

Type of Perovskite Electrode	Perovskite Preparation	Sensitivity	Linear Range	LOD	Lifetime	Applications	References
$\text{Pr}_{1.92}\text{Ba}_{0.08}\text{NiO}_{0.95}\text{Zr}_{0.05}\text{O}_{4+\delta}$ gold electrode	Citrate-nitrate Sol-gel method + calcination	101 $\mu\text{A}/\log\text{C}$ 604 $\mu\text{A}/\log\text{C}$	1.5–50 μM 0.05–7 mM	0.5 μM		Human serum	[35]
$\text{Sr}_{1.7}\text{Ca}_{0.3}\text{PdO}_3$ Graphite electrode	Glycine-nitrate method + calcination	306.9 $\mu\text{A}/\text{mM}$ 54.17 $\mu\text{A}/\text{mM}$	5 μM –1.4 mM 1.8–5.6 mM	8.45 nM	50 cycles	Human urine samples	[36]
NdNiO_3 GCE	Hydrothermal method Co-precipitation	1105.1 $\mu\text{A}/\text{mM}/\text{cm}^2$	0.0005–4.6 mM	0.3 μM	15 days	Human blood samples	[37]
$\text{Sr}_2\text{Pd}_{0.7}\text{Au}_{0.3}\text{O}_3$ Graphite electrode	Glycine-nitrate method + calcination	1.44×10^4 $\mu\text{A}/\text{mM}/\text{cm}^2$ 1639 $\mu\text{A}/\text{mM}/\text{cm}^2$	0.4–10 μM 20 μM –100 μM	2.11 nM 18.5 nM		Urine samples	[38]
$\text{La}_{0.6}\text{Sr}_{0.4}\text{Co}_{0.2}\text{Fe}_{0.8}\text{O}_{3-\delta}$	Citrate-nitrate Sol-gel method + calcination	285 $\mu\text{A}/\text{mM}/\text{cm}^2$	0–200 μM	7 μM			[31]
$\text{La}_{0.6}\text{Sr}_{0.4}\text{CoO}_{3-\delta}$ Perovskite + Nafion®/GCE	EDTA-citrate complexing sol-gel + calcination	275 $\mu\text{A}/\text{mM}/\text{cm}^2$	5–1500 μM	0.15 μM			[32]
LaNiO_3 CPE	Metal salts mixed with PVP Electrospun nanofibers	42.321 $\mu\text{A}/\text{mM}/\text{cm}^2$	1–1000 μM	0.32 μM	4 weeks		[22]
$\text{Co}_{0.4}\text{Fe}_{0.6}\text{LaO}_3$ CPE	Citrate-nitrate Sol-gel method	1013.8 $\mu\text{A}/\text{mM}/\text{cm}^2$	0.05–5 and 5–500 μM	0.01 μM	3 weeks		[29]
$\text{LaNi}_{0.6}\text{Co}_{0.4}\text{O}_3$ CPE	Sol-gel method + calcination	643 $\mu\text{A}/\text{mM}/\text{cm}^2$	0.05–200 μM	8.0 nM	20 days		[28]
$\text{LaNi}_{0.5}\text{Ti}_{0.5}\text{O}_3$ CPE	Citrate-nitrate Sol-gel method + calcination	1630 $\mu\text{A}/\text{mM}/\text{cm}^2$	0.2–20 μM 0.02–1 mM	0.07 μM	40 days	Human blood serum	[39]
$\text{La}_{0.88}\text{Sr}_{0.12}\text{MnO}_3$ CPE	Metal salts mixed with PVP Electrospun nanofibers	1111.11 $\mu\text{A}/\text{mM}/\text{cm}^2$	0.05–100 μM	31.2 nM	15 days	Serum samples	[40]
$\text{La}_{0.6}\text{Sr}_{0.4}\text{CoO}_{3-\delta}$ Perovskite + RGO + Nafion®/GCE	EDTA-citrate complexing sol-gel + calcination	330 $\mu\text{A}/\text{mM}/\text{cm}^2$	2–3350 μM	0.063 μM			[32]
$\text{LaTiO}_3\text{-Ag}_{0.1}$ GCE ECL sensor	Glycine-nitrate method + calcination	782 $\mu\text{A}/\text{mM}/\text{cm}^2$	0.1 μM –0.1 mM	2.5 nM	4 weeks	Human serum samples	[41]
$\text{LaTiO}_3\text{-Ag}_{0.2}$ GCE	Sol-gel method Butyl titanate in nitric acid + calcination	784.14 $\mu\text{A}/\text{mM}/\text{cm}^2$	2.5 μM –4 mM	0.21 μM	One month	Blood serum samples	[42]
SrPdO_3 + AuNP modified graphite electrode	Citrate-nitrate method + calcination	422.3 $\mu\text{A}/\text{mM}/\text{cm}^2$	0.1–6 mM	10.1 μM	7 weeks		[43]

The complex mechanism for the electrooxidation of glucose on $\text{La}_{0.6}\text{Sr}_{0.4}\text{CoO}_{3-\delta}$ at 0.06 V/Ag/AgCl, in 0.1 M NaOH is presented in [32] and is similar to the proposed mechanism for the electrooxidation of H_2O_2 , according to two pathways via the $\text{Co}^{3+}/\text{Co}^{4+}$ redox couple and via the LOM-OER.

The lower detection limit obtained with La-based perovskite (8 nM) is obtained with $\text{LaNi}_{0.6}\text{Co}_{0.4}\text{O}_3$ [28]. The perovskite gives also a lower detection limit for H_2O_2 (Table 1), showing the higher catalytic effect of B-site ions Ni and Co. Two La-based perovskites are associated with conductive nanomaterials such as AgNPs [41,42], leading to a very low detection limit (2.5 nM) with an Electrochemiluminescence (ECL) sensor [41].

Other lanthanide A-site ions are used, such as praseodyme [31] and neodyme [33], substituted by alkaline earth such as Ba [35]. Another used A-site ion is an alkaline earth ion, strontium [36,38,43]. The lower detection limit of 2.11 nM was obtained with $\text{Sr}_2\text{Pd}_{0.7}\text{Au}_{0.3}\text{O}_3$ [38]. SrPdO_3 is also associated with conductive nanomaterials such as AuNPs [43], which allows the selective detection of glucose in the presence of other bioactive interfering species ascorbic acid (AA), uric acid (UA), *N*-acetyl-para-aminophenol or paracetamol (APAP), and DA to be shown through linear sweep voltammetry (LSV) in the case of $\text{SrPdO}_3/\text{AuNPs}$ (Figure 4) [43].

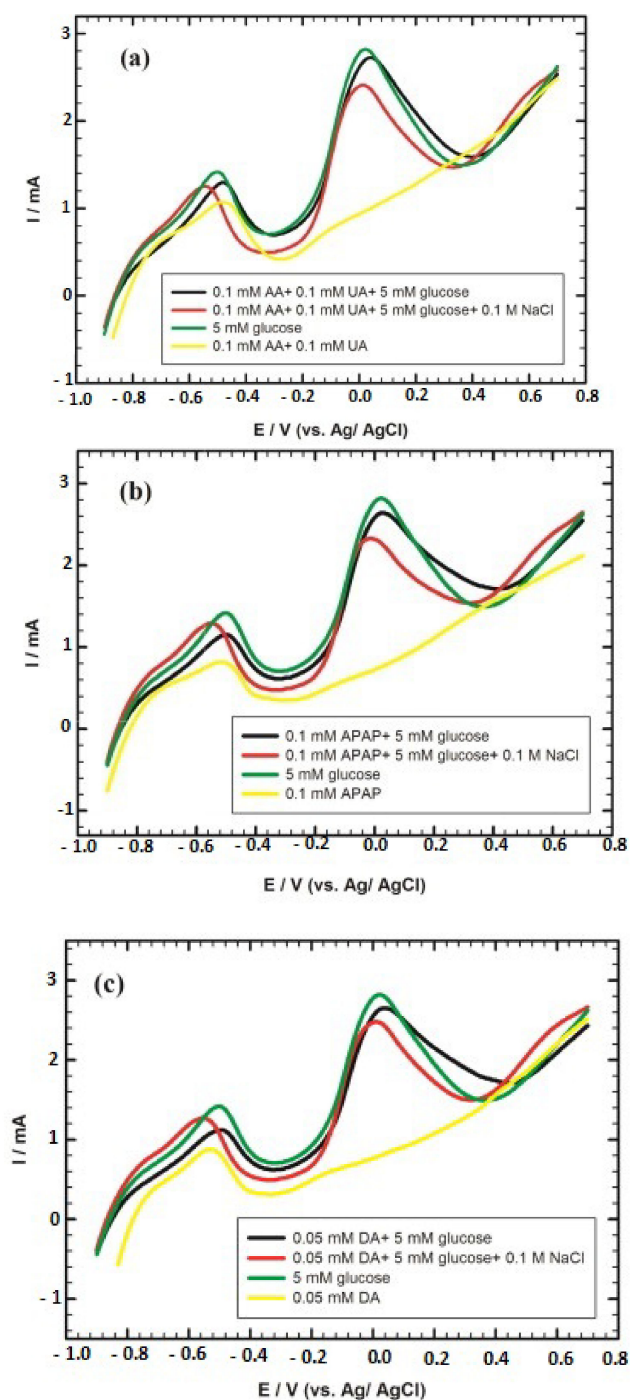


Figure 4. (a) Linear sweep voltammetry (LSV) curves of 5 mM glucose/0.1 M NaOH in the absence and the presence of 0.1 mM ascorbic acid (AA), 0.1 mM uric acid (UA) and 0.1 M NaCl at graphite/SrPdO₃/AuNPs. (b) LSV curves of 5 mM/0.1 M NaOH in the absence and the presence of 0.1 mM *N*-acetyl-para-aminophenol or paracetamol (APAP) and 0.1 M NaCl at graphite/SrPdO₃/AuNPs. (c) LSV curves of 5 mM glucose/0.1 M NaOH in the absence and the presence of 0.05 mM dopamine (DA) and 0.1 M NaCl at graphite/SrPdO₃/AuNPs [43]. Reproduced with the permission from Elsevier.

5. Perovskite-Based Electrochemical Sensors for the Detection of DA

Seventeen papers from 2014 to 2021 are devoted to the electrocatalytic detection of DA using perovskite nanomaterials (Table 3).

Table 3. Perovskite-based electrochemical sensors for the detection of DA and other bioactive molecules.

Type of Detected Molecule	Type of Perovskite Electrode Perovskite Preparation	Sensitivity	Dynamic Range	LOD	Lifetime	Applications	References
DA in the presence of ascorbic acid and uric acid	LaFeO ₃ GCE Solid state synthesis		10–100 μM 120–180 μM	10 nM	10 days	Blood samples	[21]
DA	LaFeO ₃ microspheres GCE Sol-gel method Nitrate+ ethylene glycol		0.02–1.6 μM	59 nM			[44]
DA in the presence of AA and UA	LaCoO ₃ GCE Hydrothermal process	0.033 μA/μM	1–100 μM 0.5–5 mM 0.5–5 mM	3.53 μM			[45]
DA, acetaminophen, xanthine	LaFe _{0.2} Ni _{0.8} O ₃ Carbon ceramic microelectrode Hydrothermal method Co-precipitation	0.0109 μA/μM 0.008 μA/μM 0.0274 μA/μM	6.6–131 μM 10–131 μM 3–115 μM	2.1 μM 3.2 μM 1.3 μM			[46]
DA	LaFeO ₃ Graphite powder Combustion technique		5–200 μM	600 nM	20 days		[47]
DA	LaMnO ₃ GCE Natural lemon juice– nitrate sol-gel method		1–600 μM	32 nM		Human urine saliva	[48]
DA	LaNiO ₃ Citrate + glycine method + calcination CPE	63.59 μA/mM	80 nM–20 μM	9 nM	One month	Urine and serum	[49]
Simultaneous detection of DA in the presence of ascorbic acid and uric acid	SrPdO ₃ CPE Citrate + glycine + urea method + calcination	0.88 μA/μM	7–70 μM	9.3 nM		Human urine samples	[50]
DA	NdFeO ₃ SPCE Metal salts mixed with PVP + calcination		0.5–100 μM 150–400 μM	0.27 μM		Urine	[51]
DA UA	FeTiO ₃ coprecipitation + calcination	1.56 μA/μM/cm ²	1–90 μM 1–150 μM	1.3 nM 30 nM	One week	Human serum	[52]
DA	NaNbO ₃ GCE Solvothermal method NbCl ₃ + ethanol Nb ₂ O ₅ + Na ₂ CO ₃	99 nA/nM/cm ² 77 nA/nM/cm ² 75 nA/nM/cm ²	10–50 nM 100–500 nM 1–500 μM	6.8 nM		Simulated blood samples	[53]
DA	SrTiO ₃ /GO GCE Citrate-nitrate method + calcination	0.0126 μA/μM/cm ²	0.05–531 μM	10 nM		Blood serum Urine	[54]

Table 3. Cont.

Type of Detected Molecule	Type of Perovskite Electrode Perovskite Preparation	Sensitivity	Dynamic Range	LOD	Lifetime	Applications	References
DA	β -NaFeO ₂ GCE Solid-state reaction assisted synthesis Na ₂ CO ₃ + Fe ₂ O ₃	DA 27.16 μ A/ μ M/cm ²	DA 0.010–40 μ M	DA 2.12 nM		Simulated blood samples	[55]
DA	NdFeO ₃ Nitrates + PVP + calcination		0.5–400 μ M	270 nM			[56]
DA	ZnSnO ₃ nano cube One-pot hydrothermal technique GCE		10 nM–5 μ M	2.6 nM		Blood serum	[57]
DA	CoTMPPyP/Sr ₂ Nb ₃ O ₁₀ GCE Solid-state reaction assisted synthesis		0.02–1.62 mM	7.6 μ M	30 days	Human urine	[58]
DA	CsPbBr ₃ nanocrystals encapsulated in conductive silica gel Sol-gel method		0.01–10 μ M	3 nM			[59]

The electrooxidation of DA on FeTiO₃ is depicted in Figure 5 [52]. The adsorption of DA on the FeTiO₃ surface (including the oxygen deficient sites) occurs, due to the electrostatic force of attraction. The oxidation process, with respect to the applied potential, takes place according to two pathways via the Ti³⁺/Ti⁴⁺ and Fe²⁺/Fe³⁺ redox couples and via the LOM-OER.

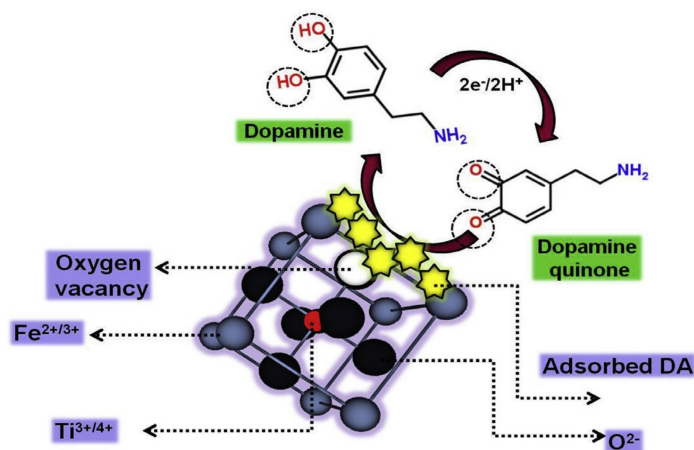


Figure 5. Electrooxidation mechanism of DA on FeTiO₃ [52]. Reproduced with the permission from Elsevier.

With La-based perovskites, the B-site ions are, as for hydrogen peroxide and glucose detection, Fe, Co, Mn, or Ni. In [49], the electrochemical detection of DA is performed with LaFeCO₃, LaCoO₃, and LaNiO₃ for the comparison of the influence of the B-site cations. The lower detection limit of 9 nM is obtained with LaNiO₃. This result was explained by the fact that the energy of the 3d electron present in Ni³⁺ is higher than those in Co³⁺ and Fe³⁺. Then, the energy of the 3d electron may become higher than that of the orbital energy (LUMO) of the analyte in the solution. Thermodynamically favorable energy transfer is then possible towards the LaNiO₃-modified electrode, better than towards the other perovskite-modified electrodes. Among other lanthanide A-site ions, it was shown that between neodymium and samarium, Nd-based perovskite (NdFeO₃) presents the lower detection limit of 270 nM [56]. Other A-site ions are alkali ions such as sodium [53,55], cesium [59], alkaline-earth ions such as strontium [50,54,58], iron ions [52], or zinc ions [57]. Associated B-site ions, involved in one of the pathways of oxidation of DA to DA hydroquinone (Figure 5), are palladium [50], titanium [52,54], niobium [53,59], iron [55], tin [57], and lead [59]. The lower detection limits (1–3 nM) are obtained with FeTiO₃ [53], β-NaFeO₂ [55], ZnSnO₃ [57], and CsPbBr₃ [59].

Apart from the sensitivity of detection, the simultaneous detection of DA in the presence of other bioactive molecules is another concern. A simultaneous detection of two neurotransmitters, DA and serotonin, in the presence of acetaminophen and tyrosine is obtained with LaNiO₃ (Figure 6) [49].

Inadequate levels of DA in human blood sera leads to neurological disorders such as Parkinson's disease, while abnormal levels of UA, xanthine, and hypoxanthine result in gout, pneumonia, and others. Therefore, the simultaneous detection of these biomarkers is of high interest. It has been obtained using electrocatalysis with β-NaFeO₂ perovskite (Figure 7) [55].

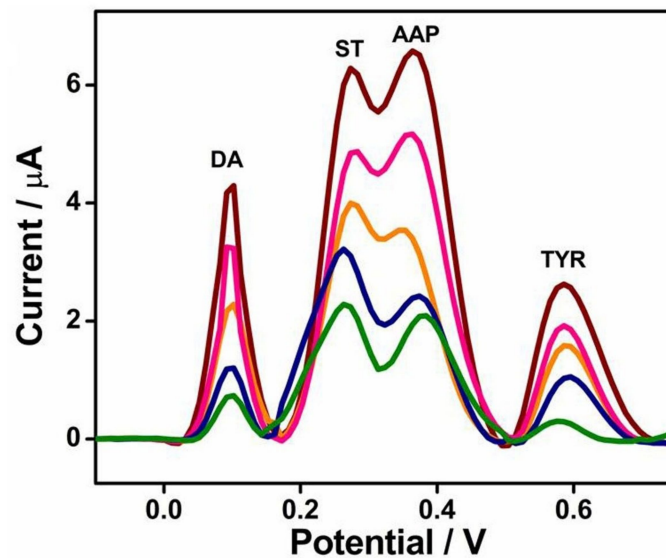


Figure 6. Interference measurement of $\text{LaNiO}_3/\text{carbon}$ paste electrode (CPE) sensor using differential pulse voltammetry (DPV) technique in 0.1 M PBS of pH 7 containing varying concentrations of DA (from green to garnet curve 0.005 to 0.045 mM), serotonin (from green to garnet curve 0.03 to 0.17 mM), acetaminophen (from green to garnet curve 0.03 to 0.09 mM), and tyrosine (from green to garnet curve 0.0008 to 0.04 mM) [49]. Reproduced with the permission from Elsevier.

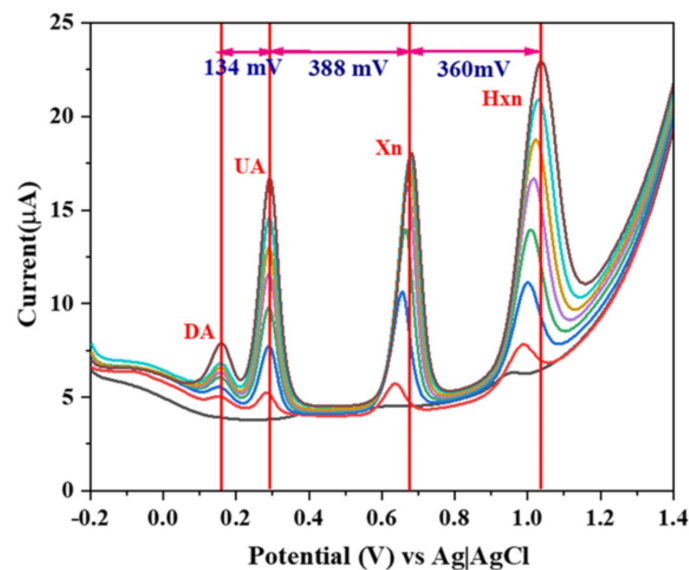


Figure 7. DPV response of a $\beta\text{-NaFeO}_2$ -modified carbon paste electrode at different concentrations of DA (from red to black curve 10 nM to 70 nM), UA (from red to black curve 5 μM to 200 μM), Xn (from red to black curve 5 μM to 200 μM), and Hxn (from red to black curve 5 μM to 200 μM) [55]. Reproduced with the permission from Elsevier.

6. Comparison of Perovskite-Based Electrochemical Sensors with Ni and Co Oxide-Based Electrochemical Sensors

Nickel oxide nanomaterials and cobalt oxide nanomaterials are also used due to their electrocatalytic properties for the detection of electroactive molecules as hydrogen peroxide, glucose, and DA. The works published in the five last years, where the oxide nanomaterials were not associated with other nanomaterials such as graphene, carbon nanotubes, or metallic nanoparticles, are presented in Table 4.

Table 4. Nickel oxide and cobalt oxide-based electrochemical sensors for the detection of bioactive molecules.

Target	Oxide Preparation Electrode	Sensitivity	Linear Range	LOD	Lifetime	Applications	References
NiO nanomaterials							
Glucose	Hydrothermal synthetic approach NiO hollow cages on a Nafion/GCE	2476.4 $\mu\text{A}/\text{mM}/\text{cm}^2$	0.1–5.0 mM	0.1 μM	8 weeks	Human serum	[60]
Glucose	NiO nanopetals on FTO/glass	3.9 $\mu\text{A}/\mu\text{M}/\text{cm}^2$	100 μM –1.2 mM	1 μM			[61]
Glucose	Sol-gel hydrothermal route NiO on ITO	24 $\mu\text{A}/\text{mM}/\text{cm}^2$	0.01–83 mM	8.1 μM			[62]
Glucose	Ultrasound-assisted anodization of nickel foils	206.9 $\mu\text{A}/\text{mM}/\text{cm}^2$	0.1–10.0 mM	1.16 μM	30 days		[63]
Glucose	Hydrothermal synthetic approach NiO on a gold electrode	1618.4 $\mu\text{A}/\text{mM}/\text{cm}^2$	0.25–3.75 mM	2.5 μM			[64]
DA	CTAB-NiO prepared by co-precipitation CPE		1–800 μM	0.68 μM		Human blood serum	[65]
DA	Hydrothermal synthetic approach NiO/ITO	0.064 $\mu\text{A}/\mu\text{M}$	0.5–5 μM	85 nM		Dopamine release from PC12 cells	[66]
DA	Electrodeposited nanoNiOx on a GCE	0.329 $\mu\text{A}/\mu\text{M}/\text{cm}^2$	80.0–800 μM	0.69 μM		Vitamin C	[67]
Co₃O₄ nanomaterials							
H ₂ O ₂	3D porous Co ₃ O ₄ on a Nafion/GCE	389.7 $\mu\text{A}/\text{mM}/\text{cm}^2$	0.4–200 μM	0.24 μM			[68]
Glucose	Hydrothermal growth of Co ₃ O ₄ nanowires on a Nafion/GCE	300.8 $\mu\text{A}/\text{mM}/\text{cm}^2$	5–570 μM	5 μM	One month	Human serum	[69]
Glucose	Hydrothermal growth of Co ₃ O ₄ nanodisks on a Nafion/GCE	27.33 $\mu\text{A}/\text{mM}/\text{cm}^2$	0.5–5.0 mM	0.8 μM		Blood serum samples	[70]
Glucose	3D porous Co ₃ O ₄ on a Nafion/GCE	471.5 $\mu\text{A}/\text{mM}/\text{cm}^2$	1 μM –12.5 mM	0.1 μM	60 days	Human serum samples	[68]

Hydrogen peroxide is detected with a 3D porous Co₃O₄/Nafion-modified GCE at 0.31 V/SCE, in a 0.1 M NaOH solution, and a detection limit of 0.24 μM is obtained [68]. A detection limit of 1 nM is obtained with a LaNi_{0.6}Co_{0.4}O₃ carbon paste electrode [28], and a detection limit of 2 nM is obtained with a Co_{0.4}Fe_{0.6}LaO₃ carbon paste electrode [29], with the voltammetric signal being obtained at 0.55 V/SCE in 0.1 M NaOH. A detection limit of 23 nM is obtained with a LaNi_{0.5}Ti_{0.5}O₃/CoFe₂O₃-modified GCE [30], and a detection limit of 35 nM is obtained with a LaNiO₃/Nafion-modified GCE [34], with the voltammetric signal being obtained at 0.6 V/SCE [30] and at −0.5 V/SCE (cathodic peak) [34] in 0.1 M NaOH. When the experimental conditions are similar, the detection limit for hydrogen peroxide obtained with lanthanum-based perovskite is lower than that obtained with cobalt oxide nanomaterials.

When glucose is detected with NiO-modified electrodes, the obtained detection limits are between 0.1 μM and 8.1 μM [60–64], with glucose being detected between 0.48 V/SCE and 0.58 V/SCE, in 10^{−4} M–0.5 M NaOH. When glucose is detected with Co₃O₄-modified electrodes, the obtained detection limits are between 0.1 μM to 5 μM [68–70], with glucose being detected between 0.47 V/SCE and 0.6 V/SCE, in 0.1–0.3 M NaOH. With a Sr₂Pd_{0.7}Au_{0.3}O₃-modified graphite electrode, a detection limit of 2.11 nM is obtained [38], and with a LaNi_{0.6}Co_{0.4}O₃ carbon paste electrode, a detection limit of 8.0 nM is obtained [28], with glucose being detected in a 0.1 M NaOH solution at −76 mV/SCE (with Sr₂Pd_{0.7}Au_{0.3}O₃) and at 0.55 V/SCE (with LaNi_{0.6}Co_{0.4}O₃). The experimental conditions for glucose detection in the presence of lanthanum-based perovskites are very close to those for glucose detection in the presence of oxide-modified electrodes, but the obtained detection limit is lower. In the presence of Pd–Au–B site strontium perovskite, the detection conditions are quite different (very low oxidation potential), and the detection limit is quite lower [38].

When DA is detected with NiO-modified electrodes, the obtained detection limits are between 85 nM and 690 nM [65–67], with DA being detected at 0.2 V/SCE, at pH between 6 and 7.4. When DA is detected with a LaNiO₃ carbon paste electrode, a detection limit of 9 nM is obtained [49], with the detection being obtained at very similar conditions at 0.1 V/SCE and pH 7. When DA is detected with a FeTiO₃-modified GCE, a detection limit of 1.3 nM is obtained [52], with the detection being obtained at very similar conditions at 0.15 V/SCE in PBS. Besides the detection limit, another point is the simultaneous detection of DA with possible interfering molecules such as AA and UA. With a LaFeO₃-modified GCE, the detection limit of DA is 10 nM, and the positions of the different anodic peaks are 0.25 V/SCE, −0.05 V/SCE, and 0.38 V/SCE for DA, AA, and UA, respectively. With NiO-modified electrodes, the anodic peak of DA is at 0.21 V/SCE, and the anodic peaks of AA and UA are at 0.02 V/SCE and at 0.32 V/SCE, respectively. When comparing the DA–AA peak distance, it comes that with a LaFeO₃-modified GCE, it is 0.30 V/SCE and with a NiO-modified electrode, it is between 0.19 V/SCE and 0.23 V/SCE, which is lower. When comparing the DA–UA peak distance, it comes that with a LaFeO₃-modified GCE, it is 0.13 V/SCE and with a NiO-modified electrode, it is 0.11 V/SCE. It appears that with a LaFeO₃-modified GCE, the DA anodic peak is more separated from the interfering peaks.

All these examples show that with lanthanum-based perovskites, with Ni or Co B-site, lower detection limits compared to with nickel and cobalt oxides are obtained and much lower detection limits could be obtained with, for instance, Sr–Pd and Fe–Ti-based perovskites, without any other nanomaterials. Moreover, with LaFeO₃, the distance between the anodic peaks of the interfering compounds can be larger.

7. Conclusions and Perspectives

A lot of ABO₃ perovskites are used for their electrocatalytic properties applied for the sensitive electrochemical detection of bioactive molecules: hydrogen peroxide, glucose, and DA. La-based perovskites, containing Ni and Co ions as B-site, present a higher sensitivity of detection, with the detection limit being in the range of 1–10 nM. The proposed mechanism for the electrooxidation of the bioactive molecules takes place in two pathways

via the B^{3+}/B^{4+} redox couple and via the LOM-OER. The experimental conditions for the hydrogen peroxide, glucose, and DA detection in the presence of lanthanum-based perovskites are very close to those for their detection in the presence of oxide-modified electrodes, but the obtained detection limit is lower due to the involved complex mechanism of detection.

The main trends for improving the analytical performance are the nanostructuring of perovskite materials (nanocrystals, nanoneedles, etc.) for increasing their specific surface areas and the association of perovskites with conductive nanomaterials such as carbon nanotubes, graphene, and metallic nanomaterials. Some perovskites are commercially available; for instance, $CsPbBr_3$ is in form of quantum dots or others are in form of powders or can be used for sputtering. They could also be easily used due to their electrocatalytic properties.

The applications of perovskite-modified electrodes are numerous, due to the large range of detectable molecules and the concerned biomedical, environmental, and agrifood fields. For limiting the environmental impact of perovskite nanomaterials and due to the scarcity and the toxicity of rare earth elements, it is necessary to recycle these elements as well as heavy metals (Ni, Co, and Pb), using solid-state extraction, for instance graphite/magnetite nanocomposites.

Author Contributions: Conceptualization, A.Z. and I.B.; resources, A.E.; writing—original draft preparation, I.B.; writing—review and editing, N.J.-R. All authors have read and agreed to the published version of the manuscript.

Funding: This research was funded by CAMPUS FRANCE, through PHC Maghreb #39382RE.

Institutional Review Board Statement: Not applicable.

Informed Consent Statement: Not applicable.

Acknowledgments: I.Boubezari thanks the government of Algeria for her work-study grant.

Conflicts of Interest: The authors declare no conflict of interest.

References

1. Vashist, S.K.; Lupta, P.B.; Yeo, L.Y.; Ozcan, A.; Luong, J.H.T. Emerging Technologies for Next-Generation Point-of-Care Testing. *Trends Biotechnol.* **2015**, *33*, 692–705. [[CrossRef](#)]
2. Wang, J. Electrochemical Glucose Biosensors. *Chem. Rev.* **2008**, *108*, 814–825. [[CrossRef](#)]
3. Szatrowski, T.P.; Nathan, C.F. Production of large amounts of hydrogen peroxide by human cells. *Cancer Res.* **1991**, *51*, 794–798.
4. Lockhart, M.J.; Smith, D. Should continuous glucose monitoring systems be offered to all patients with type 1 diabetes mellitus? *Ir. J. Med. Sci.* **2021**, 1–14, Online ahead of print. [[CrossRef](#)]
5. Sackner-Bernstein, J. Estimates of Intracellular Dopamine in Parkinson's Disease: A Systematic Review and Meta-Analysis. *J. Parkinsons Dis.* **2021**, *11*, 1011–1018. [[CrossRef](#)]
6. Zhang, Y.; Zhou, N. Electrochemical Biosensors Based on Micro-fabricated Devices for Point-of-care Testing: A Review. *Electroanalysis* **2021**, *33*, 1–17.
7. Mass, M.; Veiga, L.S.; Garate, O.; Longinotti, G.; Moya, A.; Ramón, E.; Villa, R.; Ybarra, G.; Gabriel, G. Fully Inkjet-Printed Biosensors Fabricated with a Highly Stable Ink Based on Carbon Nanotubes and Enzyme-Functionalized Nanoparticles. *Nanomaterials* **2021**, *11*, 1645. [[CrossRef](#)] [[PubMed](#)]
8. Jin, X.; Li, G.; Xu, T.; Su, L.; Yan, D.; Zhang, X. Ruthenium-based Conjugated Polymer and Metal-organic Framework Nanocomposites for Glucose Sensing. *Electroanalysis* **2021**, *33*, 1902–1910. [[CrossRef](#)]
9. Baluta, S.; Zaja, D.; Szyszka, A.; Malecha, K.; Cabaj, J. Enzymatic Platforms for Sensitive Neurotransmitter Detection. *Sensors* **2020**, *20*, 423. [[CrossRef](#)]
10. Wolfram, T.; Ellialtioglu, S. *Electronic and Optical Properties of d-Band Perovskites*; Cambridge University Press: Cambridge, UK, 2009; ISBN 9780511541292.
11. Szafraniak, B.; Fusnik, L.; Xu, J.; Gao, F.; Brudnik, A.; Rydosz, A. Semiconducting metal oxides: $SrTiO_3$, $BaTiO_3$ and $BaSrTiO_3$ in gas-sensing applications: A review. *Coatings* **2021**, *11*, 185. [[CrossRef](#)]
12. Atta, N.F.; El-Ads, E.H.; Galal, A. *Perovskites: Smart Nanomaterials for Sensory Applications in Designing Nanosensors for Chemical and Biological Applications*; Atta, N.F., Ed.; International Frequency Sensor Association Publishing: Barcelona, Spain, 2017; pp. 149–205. ISBN 978-84-697-3290-8.
13. Assirey, E.A.R. Perovskite synthesis, properties and their related biochemical and industrial application. *Saudi Pharm. J.* **2019**, *27*, 817–829. [[CrossRef](#)] [[PubMed](#)]

14. Chen, T.W.; Ramachandran, R.; Chen, S.M.; Kavitha, N.; Dinakaran, K.; Kannan, R.; Anushya, G.; Bhuvana, N.; Jeyapragasam, T.; Mariyappan, V.; et al. Developing low-cost, high performance, robust and sustainable perovskite electrocatalytic materials in the electrochemical sensors and energy sectors: "An overview". *Catalysts* **2020**, *10*, 938. [[CrossRef](#)]
15. Chen, T.W.; Ramachandran, R.; Chen, S.M.; Anushya, G.; Ramachandran, K. Graphene and perovskite-based nanocomposite for both electrochemical and gas sensor applications: An overview. *Sensors* **2020**, *20*, 6755. [[CrossRef](#)] [[PubMed](#)]
16. Thatikayala, D.; Ponnamma, D.; Sadasivuni, K.K.; Cabibihan, J.J.; Al-Ali, A.K.; Malik, R.A.; Min, B. Progress of advanced nanomaterials in the non-enzymatic electrochemical sensing of glucose and H₂O₂. *Biosensors* **2020**, *10*, 151. [[CrossRef](#)] [[PubMed](#)]
17. Jesna, G.K.; Halali, V.V.; Sanjayan, C.G.; Suvina, V.; Sakar, M.; Balakrishna, R.G. Perovskite nanomaterials as optical and electrochemical sensors. *Inorg. Chem. Front.* **2020**, *7*, 2702–2725.
18. Moure, C.; Pena, O. Recent advances in perovskites: Processing and properties. *Prog. Solid State Chem.* **2015**, *43*, 123–148. [[CrossRef](#)]
19. Deganello, F.; Marci, G.; Deganello, G. Citrate–nitrate auto-combustion synthesis of perovskite-type nanopowders: A systematic approach. *J. Eur. Ceram. Soc.* **2009**, *29*, 439–450.
20. Luque, G.L.; Ferreyra, N.F.; Leyva, A.G.; Rivas, G.A. Characterization of carbon paste electrodes modified with manganese based perovskites-type oxides from the amperometric determination of hydrogen peroxide. *Sens. Actuat. B Chem.* **2009**, *142*, 331–336. [[CrossRef](#)]
21. Vijayaraghavan, T.; Sivasubramanian, R.; Shamima Hussain, S.; Ashok, A. A facile synthesis of LaFeO₃-based perovskites and their application towards sensing of neurotransmitters. *Chem. Select* **2017**, *2*, 5570–5577. [[CrossRef](#)]
22. Wang, B.; Gu, S.; Ding, Y.; Chu, Y.; Zhang, Z.; Ba, X.; Zhang, Q.; Li, X. A novel route to prepare LaNiO₃ perovskite-type oxide nanofibers by electrospinning for glucose and hydrogen peroxide sensing. *Analyst* **2013**, *138*, 362–367. [[CrossRef](#)]
23. Anh, D.T.V.; Olthuis, W.; Bergveld, P. Sensing properties of perovskite oxide La_{1-x}Sr_xCoO_{3-δ} obtained by using pulsed laser deposition. *Sens. Actuat. B Chem.* **2004**, *103*, 165–168. [[CrossRef](#)]
24. Deganello, F.; Liotta, L.F.; Leonardi, S.G.; Neri, G. Electrochemical properties of Ce-doped SrFeO₃ perovskites-modified electrodes towards hydrogen peroxide oxidation. *Electrochim. Acta* **2016**, *190*, 939–947. [[CrossRef](#)]
25. He, J.; Zhou, W.; Sunarso, J.; Xu, X.; Zhong, Y.; Shao, Z.; Chen, X.; Zhu, H. 3D ordered macroporous SmCoO₃ perovskite for highly active and selective hydrogen peroxide detection. *Electrochim. Acta* **2018**, *260*, 372–383. [[CrossRef](#)]
26. Shimizu, Y.; Komatsu, H.; Michishita, S.; Miura, N.; Yamazo, N. Sensing characteristics of hydrogen peroxide sensor using carbon-based electrode loaded with perovskite-type oxide. *Sens. Actuat. B Chem.* **1996**, *34*, 493–498. [[CrossRef](#)]
27. Xu, D.; Li, L.; Ding, Y.; Cui, S. Electrochemical hydrogen peroxide sensors based on electrospun La_{0.7}Sr_{0.3}Mn_{0.75}Co_{0.25}O₃ nanofiber modified electrodes. *Anal. Methods* **2015**, *7*, 6083–6088. [[CrossRef](#)]
28. Zhang, Z.; Gu, S.; Ding, Y.; Jin, J. A novel nonenzymatic sensor based on LaNi_{0.6}Co_{0.4}O₃ modified electrode for hydrogen peroxide and glucose. *Anal. Chim. Acta* **2012**, *745*, 112–117. [[CrossRef](#)] [[PubMed](#)]
29. Zhang, Z.; Gu, S.; Ding, Y.; Zhang, F.; Jin, J. Determination of hydrogen peroxide and glucose using a novel sensor platform based on Co_{0.4}Fe_{0.6}LaO₃ nanoparticles. *Microchim. Acta* **2013**, *180*, 1043–1049. [[CrossRef](#)]
30. Ye, D.; Xu, Y.; Luo, L.; Ding, Y.; Wang, Y.; Liu, X.; Xing, L.; Peng, J. A novel non-enzymatic hydrogen peroxide sensor based on LaNi_{0.5}Ti_{0.5}O₃/CoFe₂O₄ modified electrode. *Colloid Surf. B Biointerfaces* **2012**, *89*, 10–14. [[CrossRef](#)]
31. Liotta, L.F.; Puleo, F.; La Parola, V.; Leonardi, S.G.; Donato, N.; Aloisio, D.; Neri, G. La_{0.6}Sr_{0.4}FeO_{3-δ} and La_{0.6}Sr_{0.4}Co_{0.2}Fe_{0.8}O_{3-δ} Perovskite materials for H₂O₂ and glucose electrochemical sensors. *Electroanalysis* **2015**, *27*, 684–692. [[CrossRef](#)]
32. He, J.; Sunarso, J.; Zhu, Y.; Zhong, Y.; Miao, J.; Zhou, W.; Shao, Z. High-performance non-enzymatic perovskite sensor for hydrogen peroxide and glucose electrochemical detection. *Sens. Actuat. B Chem.* **2017**, *244*, 482–491. [[CrossRef](#)]
33. Karuppiah, C.; Kohila rani, K.; Wang, S.F.; Devasenathipathy, R.; Yang, C.C. Dry particle coating preparation of highly conductive LaMnO₃@C composite for the oxygen reduction reaction and hydrogen peroxide sensing. *J. Taiwan Inst. Chem. Eng.* **2018**, *93*, 94–102. [[CrossRef](#)]
34. Ahmadi, E.; Mohammad Bagher Gholivand, M.B.; Karamic, C. Enzyme-less amperometric sensor manufactured using a Nafion–LaNiO₃ nanocomposite for hydrogen peroxide. *RSC Adv.* **2020**, *10*, 23457–23465. [[CrossRef](#)]
35. Boubezari, I.; Zazoua, A.; Bessueille, F.; Errachid, A.; Jaffrezic-Renault, N. Design of a new non-enzymatic sensor based on a substituted A₂BO_{4+δ} perovskite for the voltammetric detection of glucose. *Electroanalysis* **2020**, *32*, 1642–1650. [[CrossRef](#)]
36. El Ads, E.H.; Galal, A.; Atta, N.F. The effect of A-site doping in a strontium palladium perovskite and its applications for non-enzymatic glucose sensing. *RSC Adv.* **2016**, *6*, 16183–16196. [[CrossRef](#)]
37. Sivakumar, M.; Pandi, K.; Chen, S.M.; Cheng, Y.H.; Sakthivel, M. Facile synthesis of perovskite-type NdNiO₃ nanoparticles for an effective electrochemical non-enzymatic glucose biosensor. *New J. Chem.* **2017**, *41*, 11201–11207. [[CrossRef](#)]
38. Atta, N.F.; Galal, A.; El-Ads, E.H. Effect of B-site doping on Sr₂PdO₃ perovskite catalyst activity for non-enzymatic determination of glucose in biological fluids. *J. Electroanal. Chem.* **2019**, *852*, 113523. [[CrossRef](#)]
39. Wang, Y.; Xu, Y.; Luo, L.; Ding, Y.; Liu, X.; Huang, A. A novel sensitive nonenzymatic glucose sensor based on perovskite LaNi_{0.5}Ti_{0.5}O₃-modified carbon paste electrode. *Sens. Actuat. B Chem.* **2010**, *151*, 65–70. [[CrossRef](#)]
40. Xu, D.; Luo, L.; Ding, Y.; Xu, P. Sensitive electrochemical detection of glucose based on electrospun La_{0.88}Sr_{0.12}MnO₃ nanofibers modified electrode. *Anal. Biochem.* **2015**, *489*, 38–43. [[CrossRef](#)] [[PubMed](#)]
41. Jia, F.F.; Zhong, H.; Zhang, W.G.; Li, X.R.; Wang, G.Y.; Song, J.; Cheng, Z.P.; Yin, J.Z.; Guo, L.P. A novel nonenzymatic ECL glucose sensor based on perovskite LaTiO₃-Ag_{0.1} nanomaterials. *Sens. Actuat. B Chem.* **2015**, *212*, 174–182. [[CrossRef](#)]

42. Wang, Y.Z.; Zhong, H.; Li, X.M.; Jia, F.F.; Shi, Y.X.; Zhang, W.G.; Cheng, Z.P.; Zhang, L.L.; Wang, J.K. Perovskite LaTiO₃-Ag_{0.2} nanomaterials for non-enzymatic glucose sensor with high performance. *Biosens. Bioelectron.* **2013**, *48*, 56–60. [[CrossRef](#)] [[PubMed](#)]
43. El Ads, E.H.; Galal, A.; Atta, N.F. Electrochemistry of glucose at gold nanoparticles modified graphite/SrPdO₃ electrode—towards a novel non-enzymatic glucose sensor. *J. Electroanal. Chem.* **2015**, *749*, 42–52. [[CrossRef](#)]
44. Thirumalairajan, S.; Girija, K.; Mastelaro, V.R.; Ganesh, V.; Ponpandian, N. Detection of the neurotransmitter dopamine by a glassy carbon electrode modified with self-assembled perovskite LaFeO₃ microspheres made up of nanospheres. *RSC Adv.* **2014**, *4*, 25957–25962. [[CrossRef](#)]
45. Priyatharshni, S.; Tamilselvan, A.; Viswanathan, C.; Ponpandian, N. LaCoO₃ nanostructures modified glassy carbon electrode for simultaneous electrochemical detection of dopamine, ascorbic acid and uric Acid. *J. Electrochem. Soc.* **2017**, *164*, B152–B158. [[CrossRef](#)]
46. Tohidinia, M.; Sabbaghi, N.; Shaybani, S.; Noroozifar, M. Simultaneous determination of dopamine, acetaminophen and xanthine by modified carbon ceramic micro-electrode with nanosized LaFe_{0.2}Ni_{0.8}O₃ perovskite. *Anal. Bioanal. Electrochem.* **2018**, *10*, 1525–1537.
47. Kumar, Y.; Pramanik, S.; Das, D.P. Lanthanum ortho-ferrite (LaFeO₃) nano-particles based electrochemical sensor for the detection of dopamine. *Biointerface Res. Appl. Chem.* **2020**, *10*, 6182–6188.
48. Shafi, P.M.; Joseph, N.; Karthik, R.; Shim, J.J.; Bose, A.C.; Ganesh, V. Lemon juice-assisted synthesis of LaMnO₃ perovskite nanoparticles for electrochemical detection of dopamine. *Microchem. J.* **2021**, *164*, 105945. [[CrossRef](#)]
49. Thomas, J.; Anitha, P.K.; Thomas, T.; Thomas, N. The influence of B-site cation in LaBO₃ (B = Fe, Co, Ni) perovskites on the nanomolar sensing of neurotransmitters. *Sens. Actuat. B Chem.* **2021**, *332*, 129362. [[CrossRef](#)]
50. Atta, N.F.; Ali, S.M.; El Ads, E.H.; Galal, A. Nano-perovskite carbon paste composite electrode for the simultaneous determination of dopamine, ascorbic acid and uric acid. *Electrochim. Acta* **2014**, *128*, 16–24. [[CrossRef](#)]
51. Anajafi, Z.; Naseri, M.; Marini, S.; Espro, C.; Iannazzo, D.; Leonardi, S.G.; Neri, G. NdFeO₃ as a new electrocatalytic material for the electrochemical monitoring of dopamine. *Anal. Bioanal. Chem.* **2019**, *411*, 7681–7688. [[CrossRef](#)]
52. Aparna, T.K.; Sivasubramanian, R. FeTiO₃ nanohexagons based electrochemical sensor for the detection of dopamine in presence of uric acid. *Mater. Chem. Phys.* **2019**, *233*, 319–328. [[CrossRef](#)]
53. Durai, L.; Badhulika, S. A facile, solid-state reaction assisted synthesis of a berry-like NaNbO₃ perovskite structure for binder-free, highly selective sensing of dopamine in blood samples. *New J. Chem.* **2019**, *43*, 11994–12003. [[CrossRef](#)]
54. Gopi, P.K.; Muthukutty, B.; Chen, S.M.; Chen, T.W.; Liu, X.; Allothman, A.A.; Ali, M.A.; Wabaidur, S.M. Platelet-structured strontium titanate perovskite decorated on graphene oxide as a nanocatalyst for electrochemical determination of neurotransmitter dopamine. *New J. Chem.* **2020**, *44*, 18431–18441. [[CrossRef](#)]
55. Durai, L.; Badhulika, S. Facile synthesis of large area pebble-like β-NaFeO₂ perovskite for simultaneous sensing of dopamine, uric acid, xanthine and hypoxanthine in human blood. *Mater. Sci. Eng. C Biomimetic Supramol.* **2020**, *109*, 110631. [[CrossRef](#)]
56. Anajafi, Z.; Naseri, M.; Neri, G. Gas sensing and electrochemical properties of rare earthferrite, LnFeO₃ (Ln = Nd, Sm). *Ceram. Int.* **2020**, *46*, 26682–26688. [[CrossRef](#)]
57. Durai, L.; Badhulika, S. One pot hydrothermal synthesis of large area nano cube like ZnSnO₃ perovskite for simultaneous sensing of uric acid and dopamine using differential pulse voltammetry. *IEEE Sensors J.* **2020**, *20*, 13212–13219. [[CrossRef](#)]
58. Wu, S.; Sun, T.; Wang, H.; Fan, Z.; Li, L.; Fan, B.; Liu, L.; Ma, J.; Tong, Z. A sandwich-structured, layered CoTMPyP/Sr₂Nb₃O₁₀ nanocomposite for simultaneous voltammetric determination of dopamine and ascorbic acid. *J. Electroanal. Chem.* **2020**, *873*, 114403. [[CrossRef](#)]
59. Li, Z.; Kang, Q.; Chen, L.; Zhang, B.; Zou, G.; Shen, D. Enhancing aqueous stability and radiative-charge-transfer efficiency of CsPbBr₃ perovskite nanocrystals via conductive silica gel coating. *Electrochim. Acta* **2020**, *330*, 135332. [[CrossRef](#)]
60. Ibupoto, Z.H.; Nafady, A.; Soomro, R.A.; Sirajuddin Shrazi, S.T.H.; Abro, M.I.; Willander, M. Glycine-assisted synthesis of NiO hollow cage-like nanostructures for sensitive non-enzymatic glucose sensing. *RSC Adv.* **2015**, *5*, 18773–18781. [[CrossRef](#)]
61. Mishra, S.; Yogi, P.; Sagdeo, P.R.; Kumar, R. Mesoporous nickel oxide (NiO) nanopetals for ultrasensitive glucose sensing. *Nanoscale Res. Lett.* **2018**, *13*, 1–7. [[CrossRef](#)] [[PubMed](#)]
62. Pal, N.; Banerjee, S.; Bhaumik, A. A facile route for the syntheses of Ni(OH)₂ and NiO nanostructures as potential candidates for non-enzymatic glucose sensor. *J. Colloid Interface Sci.* **2018**, *516*, 121–127. [[CrossRef](#)]
63. Heyser, C.; Schrebler, R.; Grez, P. New route for the synthesis of nickel (II) oxide nanostructures and its application as non-enzymatic glucose sensor. *J. Electroanal. Chem.* **2019**, *832*, 189–195. [[CrossRef](#)]
64. Ahmad, R.; Khan, M.; Tripathy, N.; Khan, M.I.R.; Khosla, A. Hydrothermally synthesized nickel oxide nanosheets for non-enzymatic electrochemical glucose. *J. Electrochem. Soc.* **2020**, *167*, 107504. [[CrossRef](#)]
65. Reddy, S.; Swamy, B.E.K.; Ramakrishana, S.; He, L.; Jayadevappa, H. NiO nanoparticles based carbon paste as a sensor for detection of dopamine. *Int. J. Electrochem. Sci.* **2018**, *13*, 5748–5761. [[CrossRef](#)]
66. Emran, M.Y.; Shenashen, M.A.; Mekawy, M.; Azzam, A.M.; Akhtar, N.; Gomaa, H.; Selim, M.M.; Faheem, A.; El-Safty, S.A. Ultrasensitive in-vitro monitoring of monoamine neurotransmitters from dopaminergic cells. *Sens. Actuat. B Chem.* **2018**, *259*, 114–124. [[CrossRef](#)]
67. Althagafi, Z.T.; Althakafi, J.T.; Al Jahdaly, B.A.; Awad, M.I. Differential electroanalysis of dopamine in the presence of a large excess of ascorbic acid at a nickel oxide nanoparticle-modified glassy carbon electrode. *J. Sensors* **2020**, *2020*, 8873930. [[CrossRef](#)]

68. Han, L.; Yang, D.P.; Liu, A. Leaf-templated synthesis of 3D hierarchical porous cobalt oxide nanostructure as direct electrochemical biosensing interface with enhanced electrocatalysis. *Biosens. Bioelectron.* **2015**, *63*, 145–152. [[CrossRef](#)]
69. Kang, L.; He, D.; Bie, L.; Jiang, P. Nanoporous cobalt oxide nanowires for non-enzymatic electrochemical glucose detection. *Sens. Actuat. B Chem.* **2015**, *220*, 888–894. [[CrossRef](#)]
70. Soomro, R.A.; Nafady, A.; Ibupoto, Z.H.; Sirajuddin; Sherazi, S.T.H.; Willander, M.; Abro, M.I. Development of sensitive non-enzymatic glucose sensor using complex nanostructures of cobalt oxide. *Mat. Sci. Semicond. Process.* **2015**, *34*, 373–381. [[CrossRef](#)]